Adaptive approach for on-board impedance parameters and voltage estimation of lithium-ion batteries in electric vehicles

Alexander Farmann [a, c, *], Wladislaw Waag [a, c], Dirk Uwe Sauer [a, b, c]

[a] Electrochemical Energy Conversion and Storage Systems Group, Institute for Power Electronics and Electrical Drives (ISEA), RWTH Aachen University, Germany
[b] Institute for Power Generation and Storage Systems (PGS), E.ON ERC, RWTH Aachen University, Germany
[c] Jülich Aachen Research Alliance, JARA-Energy, Germany

HIGHLIGHTS

- Improved adaptive approach for on-board impedance parameters estimation.
- Consideration of current dependence of the charge transfer resistance.
- Impedance-based battery model employing two ZARC-elements.
- Validation of the proposed approach under varying temperature conditions.
- Accurate voltage estimation within an RSME range of 100 mV.

ARTICLE INFO

ABSTRACT

Robust algorithms using reduced order equivalent circuit model (ECM) for an accurate and reliable estimation of battery states in various applications become more popular. In this study, a novel adaptive, self-learning heuristic algorithm for on-board impedance parameters and voltage estimation of lithium-ion batteries (LIBs) in electric vehicles is introduced. The presented approach is verified using LIBs with different composition of chemistries (NMC/C, NMC/LTO, LFP/C) at different aging states. An impedance-based reduced order ECM incorporating ohmic resistance and a combination of a constant phase element and a resistance (so-called ZARC-element) is employed. Existing algorithms in vehicles are much more limited in the complexity of the ECMs. The algorithm is validated using seven day real vehicle data with high temperature variation including very low temperatures (from $-20\,°C$ to $+30\,°C$) at different Depth-of-Discharges (DoDs). Two possibilities to approximate both ZARC-elements with finite number of RC-elements on-board are shown and the results of the voltage estimation are compared. Moreover, the current dependence of the charge-transfer resistance is considered by employing Butler–Volmer equation. Achieved results indicate that both models yield almost the same grade of accuracy.

© 2015 Elsevier B.V. All rights reserved.

1. Introduction

In recent years the development of electric and hybrid electric vehicles as an alternative to conventional vehicles have shown enormous progress. Various programs initiated by governments and car manufacturers are introduced in order to realize the fast and reliable development of aforementioned vehicles in the coming years. Although there are new vehicle models introduced by several manufacturers ready for series production, there are still certain challenges remain to be tackled. In the course of this, energy storage system as one of the major component of the powertrain of such vehicles has become much importance. The higher energy density, light weight and higher cycle lifetime of the lithium-ion batteries (LIBs) in comparison to other electrochemical storage technologies, such as lead-acid or nickel metal hydride batteries make them to potential powerful competitor [1].

Many lithium-ion cells need to be connected in series or parallel to achieve the required vehicles power demand. Reliable and safe operation of LIBs is still a challenging issue and is of critical importance and therefore need to be ensured over the battery

---

* Corresponding author. Jaegerstr. 17-19, D-52066, Aachen, Germany.
E-mail addresses: alexander.farmann@gmail.com, batteries@isea.rwth-aachen.de (A. Farmann).

lifetime. For this purpose, so-called Battery Management System (BMS) as a key part of such systems is responsible to realize this task. Monitoring algorithms use on-board measured values, such as current, voltage, temperature as an input and estimate various states of the lithium-ion battery pack (i.e., State of Charge (SoC), State of Health (SoH), State of Function (SoF) etc.) [2]. Such algorithms should be robust and be able to cope with different external factors, such as enormous temperature variations or different load profiles. Moreover, these algorithms should prevent battery's operation in critical operating ranges to ensure the guaranteed lifetime of the battery (e.g., prevention of lithium plating, prevention of operating at very low SoCs or prevention of operating at voltages and temperatures outside of the safe operating area (SoA)) [3].

The on-board estimation of impedance parameter is often employed as a basis for an accurate state estimation. Especially it is used for prediction of the available charge or discharge power that the battery can provide or collect during vehicle's operation mode [4–6]. The estimation of impedance parameters can generally be utilized employing following three techniques [7–10]:

1. Estimation techniques based on active or passive electro-chemical impedance spectroscopy (EIS).
2. Estimation techniques based on electrochemical models.
3. Estimation techniques employing adaptive filters based on reduced order equivalent circuit model (ECM).

The first methodology applies an active or passive impedance spectroscopy to get accurate insights of the chemical processes in the LIBs. In Refs. [11,12], the application of the passive and active impedance spectroscopy for impedance parameter identification of lead-acid batteries is discussed. Furthermore, in Ref. [13], the authors use an on-board EIS measurement technique for two different LIBs using nickel manganese cobalt oxide (NMC) and lithium iron phosphate (LFP) cathode materials in a frequency range of 1–2000 Hz. The electric motor controllers are used to generate the excitation signal for the impedance measurement. The main disadvantage of such technique is that no current dependence of battery impedance can be considered using passive or active EIS under real conditions.

The second technique applies electrochemical model describing phenomena occurring in the battery during its performance, whereby each electrode of the LIB is often assumed to be a single porous spherical particle [14]. Within this type of models, diffusion, intercalation and electrochemical kinetics are considered. In Refs. [15,16], authors investigate a single particle model (SPM) employing least square methodology (LS) for estimation of actual battery capacity and actual battery impedance, which is consequently connected to SoH estimation. Furthermore, unscented Kalman filter (UKF) technique for SoC estimation is employed. As a parameter for the detection of power fade, the decrease of the effective electrolyte conductivity is considered. In Ref. [17], a more sophisticated control-oriented algorithm for the estimation of the battery impedance and solid phase diffusion time of lithium ions in the positive electrode as an indicator for SoH estimation is described. The coefficients of the third-order pade′ approximated transfer function (pade′ is used for discretization of the SPM) are related to aging relevant parameters (capacity and impedance). In fact the applicability of such models on low-cost BMS is still in primitive stage and requires to be modified mainly because of high computational effort.

To reproduce the nonlinear behavior of the battery as accurate as possible, battery model is needed that considers nonlinear effects, such as diffusion and reaction processes. The employed battery model is often combined with an adaptive technique to track the changes of the impedance characteristic of the battery as they changes over the battery lifetime [4,10,18–20]. In this context, impedance-based battery models are promising compromise between accuracy and complexity for dynamic modeling of LIBs for the usage in low-cost BMS. As a major advantage in contrary to previous mentioned techniques, their limited computational effort and their applicability in wide temperature and SoC range may be addressed.

The first simple impedance-based battery model was presented in 1947 by Randles, which includes an ohmic resistance, a charge transfer resistance, a double layer capacitance and Warburg impedance describing the diffusion processes [21]. Reviews and descriptions of different impedance-based battery models may be found in Refs. [22–24]. The more accurate the battery model is the more accurate determined battery overvoltages can be. Many different adaptive techniques are shown in the past by various authors. The common is that the battery model is used in the state-space representation. The general difference between the methods is how states and parameters of the model are estimated. Two techniques can generally be distinguished [9,25]:

1. Adaptive joint estimation technique.
2. Adaptive dual estimation technique.

Joint estimation technique applies an adaptive filter on a single vector of unknown parameters and states for their estimation. The dual estimation technique uses two filters in parallel. One filter is used for the state estimation and the other one for parameter estimation. Relevant possible adaptive filters for battery state estimation can be subdivided into the following classes:

- Methods based on least squares estimation technique,
- Methods based on the Kalman filter, similar filters and observer estimation techniques.

In Ref. [26], authors show a lumped battery model considering reaction and diffusion processes, whereas parameters of ECM are estimated by applying a Kalman filter (KF). Approaches based on more advanced KF, such as extended Kalman filter (EKF) or Sigma point Kalman filter (SPKF) within the class of KF are described in Refs. [25–33]. However, in above mentioned published techniques the current dependence of the charge transfer resistance is fully neglected and the proposed techniques are verified mainly by simple pulse tests or driving cycles performed under nominal conditions.

Within this study a sophisticated ECM employing two ZARC elements (i.e., when the double layer capacitance in RC-element is replaced by a constant phase element (CPE)), ohmic resistance and a voltage source is investigated. Both of the ZARC elements are approximated on-board by a finite number of RC-elements (3 RC and 5 RC). Moreover, a recursive approach, so-called enhanced varied parameters approach (EVPA) is applied for an on-board impedance parameters estimation. The combination of the implemented nonlinear dynamic battery model and the adaptive filter for impedance parameter estimation yields very high voltage estimation accuracy. Thus, developed algorithm can be further used to estimate battery's states, such as voltage-based SoC or battery's SoH.

The remainder of this study is organized as follows: In Section 2, the functionality and basic idea of the employed adaptive filter is discussed. Based on the presented basics of the parameter estimation approach, the implemented reduced order ECM is discussed in Section 3. In Section 4, the proposed approach is validated by using three LIBs with different chemistries employing real vehicle data gathered from an EV-prototype. Finally, this work is

summarized and the applicability of the algorithm in the field is examined in the conclusion.

2. EVPA technique for impedance parameters estimation

For on-board estimation of the impedance parameters a recursive algorithm, so-called enhanced varied parameters approach is used as a basis. This algorithm is depicted in detail in our previous work [34]. The algorithm is able to adapt each adaptive parameter to particular battery's aging state and works accurately in a wide temperature range.

In the first step, the algorithm is initialized by so-called adaptive characteristic maps (ACM) for given temperature and SoC. For each adaptive parameter an ACM is implemented which is based on a polynomial approximation (i.e., 2nd order polynomial function). Dynamic ACMs ensure the tracking of impedance parameters change over battery's lifetime and keep the extracted parameters in memory. Each individual model parameter is extracted by means of electrochemical impedance spectroscopy (EIS) or hybrid pulse power characterization (HPPC) in the laboratory for a new LIB.

The underlying idea of the parameter estimation algorithm is the combination of certain values of average LIB parameters within a parameter set P for a simplified nonlinear ECM consisting of an ohmic resistance and one RC-element (R_0, R_1, k_I, C) for example $P = \{R_0 = 0.8 \text{ m}\Omega, R_1 = 1 \text{ m}\Omega, C = 200 \text{ F and } k_I = 0.01 \text{ A}^{-1}\}$. The battery load profile is then divided into short evaluation periods with a duration of approximately twenty seconds each (e.g., $k = 200$ values at sampling frequency of 10 Hz). During each evaluation period S different parameter sets (P_1, P_2, ... P_S) are generated and then S battery voltages at each sample step k during this period are calculated using the measured battery current with these parameter sets. It is assumed that during the evaluation period the OCV remains constant. The decision for starting and terminating of each of the evaluation periods is made as follows:

- First, it is verified whether the current through the capacitance over a short period of time is low (i.e., $I_C < I_{C,max}$ for Δt_C). The definition of this criterion is important, since the battery voltage can only be calculated when the previous V_C is known and at the same time the impact of the previous history on the battery voltage needs to be minimized. Moreover, since high current fluctuations in the profile allows gathering more information about the battery impedance, it is necessary to evaluate current fluctuation.
- Second, when the conditions mentioned above are fulfilled and the current profile for a pre-defined time range is evaluated, the evaluation period can be terminated and preferably the next evaluation directly begins.

This is a straight forward recursive technique. The estimated voltages are then compared to the measured battery voltage. The parameter set which results in the lowest quadratic voltage deviation (F_{Cost}) between the measured and the calculated voltage (Eq. (1)) is selected as the ideal parameter set and then used as a basis to generate parameter sets for the next evaluation period.

$$F_{Cost} = \sum_{n=1}^{k} \left(V_{meas,n} - V_{sim,n}\right)^2 \tag{1}$$

Generally, in BMS applications a compromise between accurate reproduction of battery's non-linear behavior and a low computational effort needs to be achieved. In comparison to our previous work [34] an improvement regarding the amount of the parameters required to be compared and determined is achieved. This yields

almost the same grade of accuracy by parameter estimation and fast convergence of each adaptive parameter. Moreover, the simplification allows the contribution of more complex nonlinear models.

The cost function in Eq. (1) is calculated for the initial parameter set and for parameter sets containing each time one different value of one of the parameters. Each parameter is varied in positive and negative directions. This means that for n adaptive parameters, only 2n, instead of 3^n calculations as proposed in Ref. [34] need to be performed which decrease the computational effort enormous. For example, in case of parameter R_0 the coefficient (Δ_1) is used to calculate two variations of this parameter value as follows: $R_0 + (R_0 \cdot \Delta_1)$ and $R_0 - (R_0 \cdot \Delta_1)$. The coefficient Δ_n is implemented as a variable, which may changes during each iteration period in order to accelerate the parameter convergence. In general, when the parameter adaption is stable, its value remains constant. It needs to be emphasized that the width of Δ_n plays a major role in order to ensure the parameter's convergence in a correct direction. Choosing high initial values lead consequently to wrong results and the parameter might be converges to the wrong direction. Therefore, it is recommended to explore initial values yielding accurate results for each of parameters during offline tests first.

3. Dynamic battery modeling

As discussed in the introduction, realizing a battery model which considers all the electro-chemical processes occurring in the LIB during its operation or even in the relaxation phase is a very challenging task. The exact replica of all the electrochemical processes in the LIB is rarely feasible due to the lack of knowledge and insight of various processes and the cell behavior under different conditions. At the same time, considering the limited computational capability of applications such as BMS makes reducing the model parameters to minimum by trying to depict the processes as accurate as possible necessary. In this context, presented battery models including an ohmic resistance and one RC-element, as shown for an example in our previous work [34] or more advanced models using two RC-elements meet usually the first goal, particularly low computational effort. However, they often lead to unsatisfied results, when their usage in a wide frequency (e.g., when voltage prediction in time horizon of some seconds needs to be performed etc.) and SoC range (especially low SoCs) is required.

Therefore, within this study a more sophisticated ECM incorporating an ohmic resistance, two ZARC-elements and open circuit voltage (OCV) connected in series (Fig. 1) is employed [11], [35,36]. First ZARC-element corresponds mainly to reaction processes occurring in the interface between electrode and electrolyte and the second ZARC-element corresponds to diffusion and adsorption processes occurring mainly at low frequencies in electrodes.

Furthermore, the impedance spectrum of a new LIB using NMC cathode material and graphite in the anode measured at room temperature (23 °C) is illustrated in Fig. 1. Area A shows the inductive behavior of battery at very high frequencies (>1000 Hz), which depends mainly on geometry and winding and can generally be neglected for BMS applications since it does not contain information about electrochemical state of the battery. Area B corresponds to an ohmic resistance (approximately at 500 Hz) [18]. Ohmic resistance is determined when the impedance spectrum crosses the real axis of the Nyquist plot:

$$R_0 = Re(\underline{Z}). \tag{2}$$

Part C, represents the reaction processes, whereas diffusion processes can be extracted from part D by observing the so-called diffusion ast at low frequencies (frequencies below approximately 10 Hz).
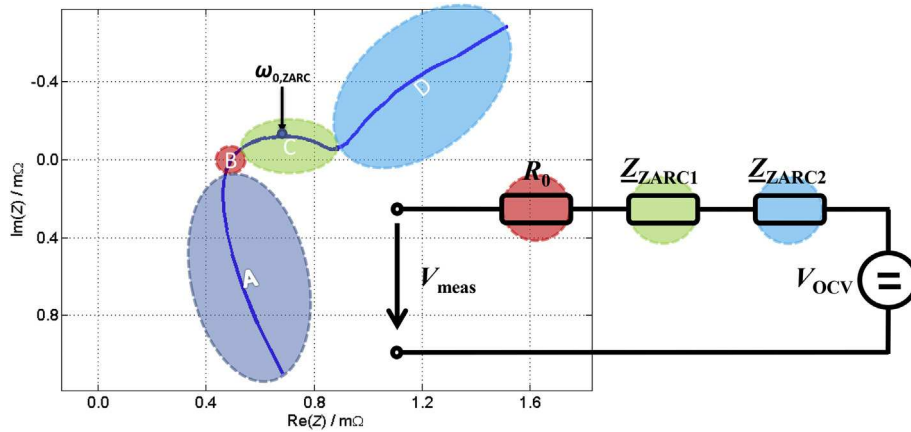
Fig. 1. Equivalent circuit model employed in this study and an example of nyquist diagram of a new LIB (NMC/C) measured at 23 °C and SoC = 50% using galvanostatic impedance measurement methodology (5000 Hz < $f$meas<1 mHz).

CPE can be described as a generalized capacitive element of a ZARC-element, while its impedance is determined as follows:

$$\underline{Z}_{CPE} = \frac{1}{A \cdot (j\omega)^\xi} \quad 0 < \xi \le 1 \tag{3}$$

where A, so-called generalized capacitance corresponds to the magnitude of CPE and ξ, so-called depression factor corresponds to depression of semi-circles in the impedance spectrum. If $\xi = 1$, CPE would be equal as a normal double layer capacitance in Randles circuit and the ZARC-element is equal to a simple RC-element. The $\xi = 0.5$ would results in $-45°$ branch in measured impedance spectrum referring to the diffusion ast of the impedance spectrum (part D in Fig. 1). If $\xi = 0$, a purely resistive behavior of a ZARC-element is derived.

The frequency at which the imaginary part of the semicircle reaches its minimum can be determined as follows (Fig. 1):

$$\omega_{0,Zarc} = \left(\frac{1}{A \cdot R}\right)^{1/\xi} = \omega_{0,RC} = \frac{1}{C_{RC} \cdot R} \tag{4}$$

Thereafter, the impedance of each ZARC-element can be analytically determined:

$$\underline{Z}_{Zarc} = \frac{R}{R \cdot A \cdot (j\omega)^\xi + 1} \quad 0 < \xi < 1 \tag{5}$$

Accordingly, impedance of the investigated ECM presented in Fig. 1 is calculated as follows:

$$\underline{Z} = R_0 + \frac{R_1}{A_1 \cdot R_1 \cdot (j\omega)^{\xi_1} + 1} + \frac{R_2}{A_2 \cdot R_2 \cdot (j\omega)^{\xi_2} + 1} \tag{6}$$

3.1. Optimized equivalent circuit model

In order to derive a ZARC-element in time domain, each individual ZARC-element is approximated by means of finite numbers of RC-elements as proposed in Ref. [35].

A well compromise between efficiency and high accuracy can be met by approximation of each ZARC-element employing three (3 RC model) or five RC-elements (5 RC model). Within this study both of these approximation's possibilities are implemented and investigated. In the following subsections the derivation techniques for both models are discussed in detail.

3.2. Approximation of the ZARC-element by means of 3 RC elements

The first assumption for the 3 RC model is the equality of RC-elements resistances.

$$R_{Zarc,k_i} = R_{Zarc,k_1} = R_{Zarc,k_2} = R_{Zarc,k_3} \tag{7}$$

$$R_{Zarc,k_1} + R_{Zarc,k_2} + R_{Zarc,k_3} = \frac{R_{Zarc,k}}{3} \tag{8}$$

$$C_{Zarc,k_1} = \frac{C_{Zarc,k_2}}{f(\xi)} \tag{9}$$

$$C_{Zarc,k_2} = \frac{1}{\omega_0 \cdot \frac{R_{Zarc,k_2}}{3}} \tag{10}$$

$$C_{Zarc,k_3} = C_{Zarc,k_2} \cdot f(\xi) \tag{11}$$

In Ref. [10] [18], values between 2 F and 50 F for LIBs using NMC in the cathode and graphite in the anode for different temperatures are extracted. $f(\xi)$ acts as a factor for depression of the semi-circles in Nyquist plot. In Table 1 corresponding values of $f(\xi)$ for 3 RC models are given.

3.3. Approximation of the ZARC-element by means of 3 RC elements

Alternatively, the ZARC-element can be approximated by means of 5 RC-elements more accurately [35]. The frequency of the middle semicircle (index 3) is assumed to be the same as the frequency of corresponding ZARC element. Accordingly, the corresponding resistance can be determined as follows:

$$R_{Zarc,k_3} = f_1(\xi) \cdot R_{Zarc,i} \cdot \frac{\sin\left(\frac{\pi}{2} \cdot \xi\right)}{1 + \cos\left(\frac{\pi}{2} \cdot \xi\right)} \tag{12}$$

$$C_{Zarc,k_3} = \frac{1}{\omega_{0,Zarc} \cdot R_{Zarc,k_3}} \tag{13}$$

Furthermore, for the sake of simplicity the resistances of two neighboring semicircles (two and four) are assumed to be equal. The associated formulas for the determination of resistances and capacitances are shown in Eq. 14–16.

Table 1
Optimization factors for approximation of a ZARC-element by 3 RC-elements.

ξ	0.4	0.45	0.5	0.55	0.6	0.65	0.7	0.75	0.8	0.85	0.9	0.95	0.99	1
$f(\xi)$	8.69	8.69	8.69	8.69	8.69	6.60	5.14	4.08	3.29	2.66	2.15	1.68	1.25	1

$$R_{\mathrm{Zarc,k_2}} = R_{\mathrm{Zarc,k_4}} = f_2(\xi) \cdot \left(\frac{R_i - R_{\mathrm{Zarc,k_3}}}{2} \right) \tag{14}$$

$$C_{\mathrm{Zarc,k_2}} = \frac{1}{\omega_{\mathrm{0Zarc,i}} \cdot f_3(\xi) \cdot R_{\mathrm{Zarc,i_2}}} \tag{15}$$

$$C_{\mathrm{Zarc,k_4}} = \frac{1}{\omega_{\mathrm{0Zarc,i}} \cdot f_3(\xi) \cdot R_{\mathrm{Zarc,i_4}}} \tag{16}$$

Two remaining semicircles can be determined assuming that the diameter of resistances one and five are equal ($R_{\mathrm{Zarc,k1}} = R_{\mathrm{Zarc,k5}}$). The determination of resistances and corresponding capacitances is shown in Eq. 17–19:

$$R_{\mathrm{Zarc,k_1}} = R_{\mathrm{Zarc,k_5}} = \left(\frac{R_i - R_{\mathrm{Zarc,k_3}} - R_{\mathrm{Zarc,k_2}} - R_{\mathrm{Zarc,k_4}}}{2} \right) \tag{17}$$

$$C_{\mathrm{Zarc,k_1}} = \frac{1}{\omega_{\mathrm{0Zarc,k}} \cdot f_3(\xi) \cdot R_{\mathrm{Zarc,k_1}}} \tag{18}$$

$$C_{\mathrm{Zarc,k_5}} = \frac{1}{\omega_{\mathrm{0Zarc,k}} \cdot f_3(\xi) \cdot R_{\mathrm{Zarc,k_5}}} \tag{19}$$

In Table 2, implemented values for depression factors are given. The values from Tables 1 and 2 are then used as a simple look-up table in the model.

The minimum of the imaginary part at frequency ω_0 (Eq. (3)) from the semi-circle can be determined by Eq. (20).

$$\min(\mathrm{Im}(\underline{Z})) = -R \cdot \frac{\left(\sin\left(\frac{\Pi}{2} \cdot \xi \right) \right)}{\left(1 + \cos\left(\frac{\Pi}{2} \cdot \xi \right) \right)} \tag{20}$$

The derivation of battery voltage in time-discrete form for both models is shown in Appendix A.

3.4. Physical meaning of the impedance parameters of the employed battery model

Each individual element of the employed battery model represents various electrochemical processes in the battery occurring in different frequency ranges. So far the battery is under load (charging or discharging), measured battery voltage differs from its voltage in equilibrium state (Eq. (21)) [37,38]. This difference is equal to sum of the battery overvoltages occurring due to charge transfer processes, diffusion (including migration and convection processes) and the ohmic voltage drop:

$$V_{\mathrm{meas}} - V_{\mathrm{ocv}} = \Delta V_{\mathrm{ohmic}} + \Delta V_{\mathrm{ct}} + \Delta V_{\mathrm{diff}} \tag{21}$$

Accordingly, measured battery voltage in the investigated ECM is equal to the sum of the resulting overvoltages (determined by ZARC-elements) and the OCV determined as follows:

$$V_{\mathrm{meas}} = V_{\mathrm{ocv}} + V_{\mathrm{R0}} + V_{\mathrm{Zarc,1}} + V_{\mathrm{Zarc,2}} \tag{22}$$

3.4.1. Ohmic resistance (R_0)

R_0 or so-called ohmic resistance corresponds to resistive contribution of electrolyte, poles, corrosion, conductors, and active mass [37], [39]. The ohmic resistance of the battery is linear and current independent; therefore the voltage drop can be calculated simply by applying ohm's law Eq. (23):

$$V_{\mathrm{R0}} = R_0 \cdot I \tag{23}$$

Independent of battery type, ohmic resistance shows a high dependence on battery's temperature due to ionic conductivity of the electrolyte and changes significantly over the battery lifetime [18], [40,41]. Therefore, R_0 is often used alone or in combination with charge transfer resistance as an indicator for SoH and remaining useful lifetime (RUL) estimation of the battery.

3.4.2. Charge transfer overvoltage (ΔV_{ct})

Charge transfer processes in batteries can be divided into the following two types: Homogenous or heterogeneous charge transfer processes [37]. Homogenous charge transfer corresponds to charge carrier (ion) exchange in electrolyte and second type corresponds to charge transfer between ions in electrolyte and ions in the electrode.

Charge transfer overvoltage is determined when the difference between the amount of lithium-ions during oxidation and reduction at both electrodes is not zero and the LIB is being charged or discharged. The correlation between current density and ΔV_{ct} is described by employing a Butler–Volmer equation [42]:

$$i = i_0 \cdot \left\{ \exp\left(\frac{\alpha_{\mathrm{anodic}} \cdot n \cdot F}{R \cdot T} \cdot \Delta V_{\mathrm{ct}} \right) - \exp\left(-\frac{\alpha_{\mathrm{cathodic}} \cdot n \cdot F}{R \cdot T} \cdot \Delta V_{\mathrm{ct}} \right) \right\} \tag{24}$$

When the effective internal surface A_{eff} is considered, the multiplication of the current density and the effective internal surface is equal to the current which flows into the electrodes ($I = i.A_{\mathrm{eff}}$). Accordingly, Eq. (24) can be rewritten as follows:

$$I = I_0 \cdot \left\{ \exp\left(\frac{\alpha_{\mathrm{anodic}} \cdot n \cdot F}{R \cdot T} \cdot \Delta V_{\mathrm{ct}} \right) - \exp\left(-\frac{\alpha_{\mathrm{cathodic}} \cdot n \cdot F}{R \cdot T} \cdot \Delta V_{\mathrm{ct}} \right) \right\} \tag{25}$$

A_{eff} changes over the battery lifetime which mainly occurs due to the decreasing of effective surface because of SEI formation on the anode. The factor I_0 denotes the exchange current density which shows a linear dependence on the concentration of the reactants and is respectively high temperature dependent. n is equal

Table 2
Optimization factors for approximation of the ZARC-element by 5 RC-elements.

ξ	0.45	0.5	0.55	0.6	0.65	0.7	0.75	0.8	0.85	0.9	0.95	0.99
$f_1(\xi)$	0.939	0.906	0.891	0.869	0.85	0.837	0.831	0.833	0.847	0.9876	0.923	0.998
$f_2(\xi)$	0.641	0.670	0.708	0.733	0.754	0.772	0.788	0.804	0.819	0.835	0.85	0.863
$f_3(\xi)$	13.141	10.886	9.661	8.331	7.15	6.176	5.352	4.675	4.112	3.634	3.218	2.855

to the involved electrons in reaction ($n = 1$ for LIBs), T is the absolute battery temperature in Kelvin, F is the Faraday constant and R is universal gas constant. α or a so-called symmetry factor refers to the charge (reduction) or discharge (oxidation) processes in the electrode (i.e., $\alpha_{\text{anodic}} + \alpha_{\text{cathodic}} = 1$). If it is assumed that both reaction processes are at the same speed (that is an simplification), which means that $\alpha = 0.5\alpha = 0.5$, then the Butler–Volmer equation can be solved analytically [39,40]:

$$I = 2I_0 \sinh\left(\frac{nF}{2RT} \cdot \Delta V_{\text{ct}}\right) \tag{26}$$

After some simple mathematical formulations the current dependence of the charge transfer resistance ($R_{\text{Zarc,1}}$) is derived as follows [10,34]:

$$R_{\text{Zarc,1}}(I_R) = R_{\text{Zarc,0}} \cdot \left(\frac{\ln\left(k_I \cdot I_R(t) + \sqrt{(k_I \cdot I_R(t))^2 + 1}\right)}{k_I \cdot I_R(t)}\right) \tag{27}$$

with k_I:

$$k_I = \frac{1}{2 \cdot I_0}\left[\text{A}^{-1}\right]. \tag{28}$$

k_I describes the behavior of the effective internal surface and the exchange current density (Eq. (28)) which becomes significant when the battery is aged or when it is operated at low temperatures as discussed earlier on. In Ref. [34] we have shown how the consideration of k_I improves the voltage estimation accuracy.

Eq. (25) is further simplified for high currents by means of so-called Tafel equation, which consequently decrease the computational effort by neglecting second exponential term. After some simple mathematical conversions defining $K = \propto \cdot F/R \cdot T$, charge transfer resistance for high discharge current rates (assumed to be I $<= -2$C) is determined:

$$R_{\text{Zarc,1}}(I) = \frac{\ln(2 \cdot I \cdot k_I)}{K_I \cdot I} \tag{29}$$

In order to avoid singularities, factor $R_{\text{Zarc,0}}$ is employed which is equal to the charge transfer resistance at $I_R = 0$ A, determined by L'hopital's rule.

3.4.3. Diffusion overvoltage (ΔV_{diff})

Concentration gradient occurring during the transportation of reacting species by charging or discharging of the battery leads to diffusion overvoltage, Generally, diffusion processes are described by the Fick's law [36,38]. In this study, the second ZARC-element is used to approximate diffusion processes occurring in the electrodes at low frequencies (below approximately 10 Hz). Consideration of diffusion overvoltage becomes essential, when battery voltage need to be predicted at higher time horizon (e.g., $\Delta t \geq 5$ s).

3.4.4. Open circuit voltage (V_{OCV})

OCV corresponds to the battery voltage, when the battery is not under load and the equilibrium state is reached. For BMS applications, the correlation between SoC and OCV is often employed as a supporting technique along with ampere-hour balancing technique to estimate battery's SoC. For LIBs using NMC or nickel-cobalt oxide (NCA) cathode materials the steep OCV curve over the whole SoC range allows an accurate SoC estimation, whereas the hysteresis effect is negligible in wide SoC region [10,43]. However, for LIBs using LFP in the cathode, due to the more emphasized hysteresis effect over a wide SoC range (i.e., 30%–80%), a separate hysteresis

model is required which depicts the difference between charged and discharged voltage accurately [43,44].

OCV depends mainly on current and temperature of the LIB since the free enthalpy correlates with lithium-ion concentration in the electrodes and it changes over battery lifetime [10,45]. Because of the self-discharge of the LIBs and long time required until the side reactions are finished, the OCV measured at the battery terminal is not equal to equilibrium voltage, so-called electro motive force [11]. Within this study, OCV is determined from the implemented ECM (Eq. (30)) on-board assuming that OCV does not change significantly between two sampling points. This allows dealing with above mentioned complexities of OCV determination instead of using for example static tables filled with OCV values of LIBs in new state.

$$V_{\text{OCV}}(k) = V_{\text{meas}}(k-1) - R_0 \cdot I(k-1) - V_{\text{Zarc,1}}(k-1) \\ - V_{\text{Zarc,2}}(k-1) \tag{30}$$

4. Results and discussion

In the previous sections, basic idea behind the implemented algorithm and the battery model is described. Often, the proposed battery monitoring techniques in the literature are validated under nominal conditions, such as constant temperature (e.g., room temperature) or by performing simple HPPC tests. However, loads which the battery pack are exposed to in the field differs significantly from the ones measured under nominal conditions in the laboratory. Hence, it is necessary to keep in mind that the developed algorithms are supposed to work accurately over years and be robust under various conditions. The robustness of the monitoring algorithms can only be examined, when long-term performance tests employing real vehicle data's for different operation conditions (e.g., highway or city, defensive or aggressive driving's mode) are applied.

Within our study a validation data set extracted from a prototype electric vehicle using a LIB battery pack is investigated. For this purpose, totally 39 driving cycles from ten different drivers consisting various driving types in a time range of one week are recorded. Extracted driving cycles are then applied to LIBs on the test-bench (temperature chambers manufactured by the company BINDER GmbH in Tuttlingen, Germany and Digatron BTS-600 manufactured by the company Digatron Power Electronics GmbH in Aachen, Germany).

The measurement accuracy of the test bench is given in Table 3:

In Fig. 2, one of the employed power profiles is exemplary shown. It is worth noting that the negative power value means discharging and the positive power charging the battery.

LIBs with different chemistries and at different aging states are investigated to show the applicability of the employed algorithm on different LIBs. In Table 4 the investigated LIBs and their individual specifications are given.

A particular emphasize during experimental tests with regard to the validation of the used algorithm is put on the following factors:

1. Wide SoC range is investigated.
2. Extreme temperature variation between driving cycles in a range of (-20 °C … -5 °C … $+10$ °C … 30 °C) is performed.

In Fig. 3, the relative distribution of temperature and SoC of the investigated driving cycles for each LIB is presented.

Determined voltage difference over the whole driving cycle is used as reference indicating the accurate impedance parameters and battery's voltage estimation respectively:

Table 3
Characteristic of the test-bench setup.

Characteristic	Maximam measurement inaccuracy	Available measurement range
Voltage measurement	±5 mV	[0 … 5] V
Current measurement	±100 mA	[−200 … +200] A
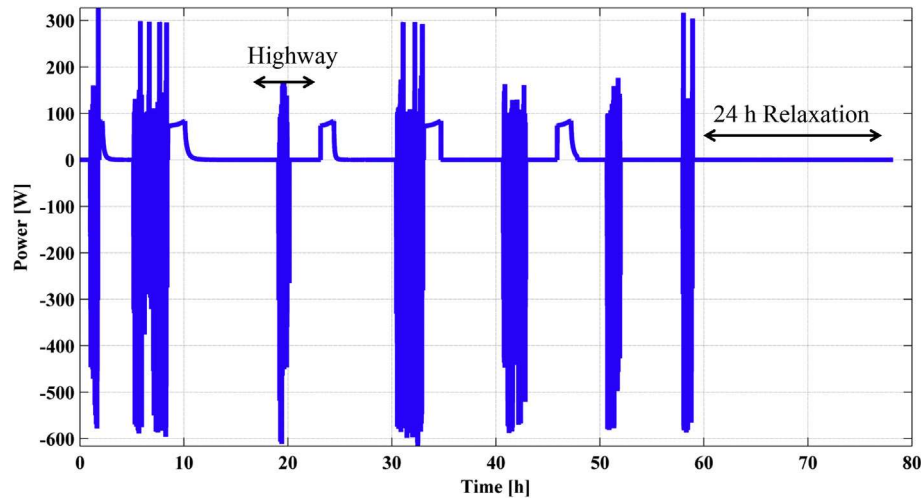
Fig. 2. An example of the measured real seven day vehicle data.

Table 4
Specification of the investigated lithium-ion batteries.

Cell type	Nominal capacity [Ah]	Actual capacity [Ah]	Nominal voltage [V]	Upper voltage limit [V]	Lower voltage limit [V]
NMC/C	40	42.3	3.7	4.2	2.7
NMC/LTO	20	20	2.3	2.7	1.5
LFP/C	8	7.0	3.2	3.7	2.0

$$\Delta V = \frac{(V_{\text{measured}} - V_{\text{sim}})}{V_{\text{nominal}}} \tag{31}$$

where ΔV refers to the normalized deviation between the measured and simulated cell voltage for a predefined amount of on-board stored voltages ($k = 200$). In Fig. 4, measured and simulated battery's voltage (including estimated overvoltages and OCV), measured temperature and the reference SoC over the whole driving cycle for NMC/C LIB are illustrated.

As discussed in Section 3, the proposed model consists of totally eight adaptive parameters {R_0, $R_{\text{Zarc,1}}$, $R_{\text{Zarc,2}}$, $A_{\text{Zarc,1}}$, $A_{\text{Zarc,2}}$, $\xi_{\text{Zarc,1}}$, $\xi_{\text{Zarc,1}}$, k_1}. These parameters are highly temperature and SoC dependent and changes over battery lifetime as shown in Ref. [10] [18], [19]. This makes the usage of an adaptive self-learning algorithm that is able to track the changes of impedance parameters over the vehicle operating period necessary.

In Fig. 5 the adaption process of the impedance parameters for an example of the driving cycle shown in Fig. 4 is illustrated. The adaption of the impedance parameters during temperature and SoC change is observable.

In order to verify the performance of each ECM, the influence of the following three factors on the accuracy of the applied ECM by estimating battery's voltage (according to Eq. (31)) is considered:

- Impact of battery's SoC on voltage estimation accuracy,
- Impact of battery's temperature on voltage estimation accuracy,
- Impact of applied current on voltage estimation accuracy.

4.1. Influence of SoC on voltage estimation accuracy

In Fig. 6a, the distribution of voltage estimation error (determined as described in Eq. (31)) for both investigated ECMs and for each LIB over the SoC range is illustrated. Due to the fact, that the distribution of the SoC range differs for of each driving cycles, the readers are referred to Fig. 3 for comparison reasons. The accuracy analysis of the ECMs is performed, while derived maximum and minimum voltage estimation error for each manifold 10% SoC range (0–10%, 10%–20%, 20%–30% etc.) is determined. Moreover, derived average voltage estimation error for each of mentioned SoC ranges are used in order to analyze the influence of the battery SoC on the estimated voltage.

As a result, an increase of estimation error at very low and high SoC ranges, especially for LIBs (NMC/C and LFP/C) is observed. Two effects may mainly contribute to this result; i: Because of large pronounced influence of diffusion processes at high and low SoC ranges which cannot be determined fully either by employing the second ZARC-element.[1] ii: High change of OCV in the aforementioned SoC ranges influences also the estimation accuracy of the battery voltage. As a consequence, when the dependence of OCV on SoC is known and the SoC is determined by any other algorithm, the

---

[1] To improve the estimation accuracy, additionally a third non-adaptive ZARC-element or a simple RC-element can be implemented which may only be switched on, when battery is operated at very low or very high SoC range (e.g., SoC < 20% or SoC > 90%). For simplicity reasons, corresponding parameters may be obtained offline from laboratory measurements for various temperatures and SoC.
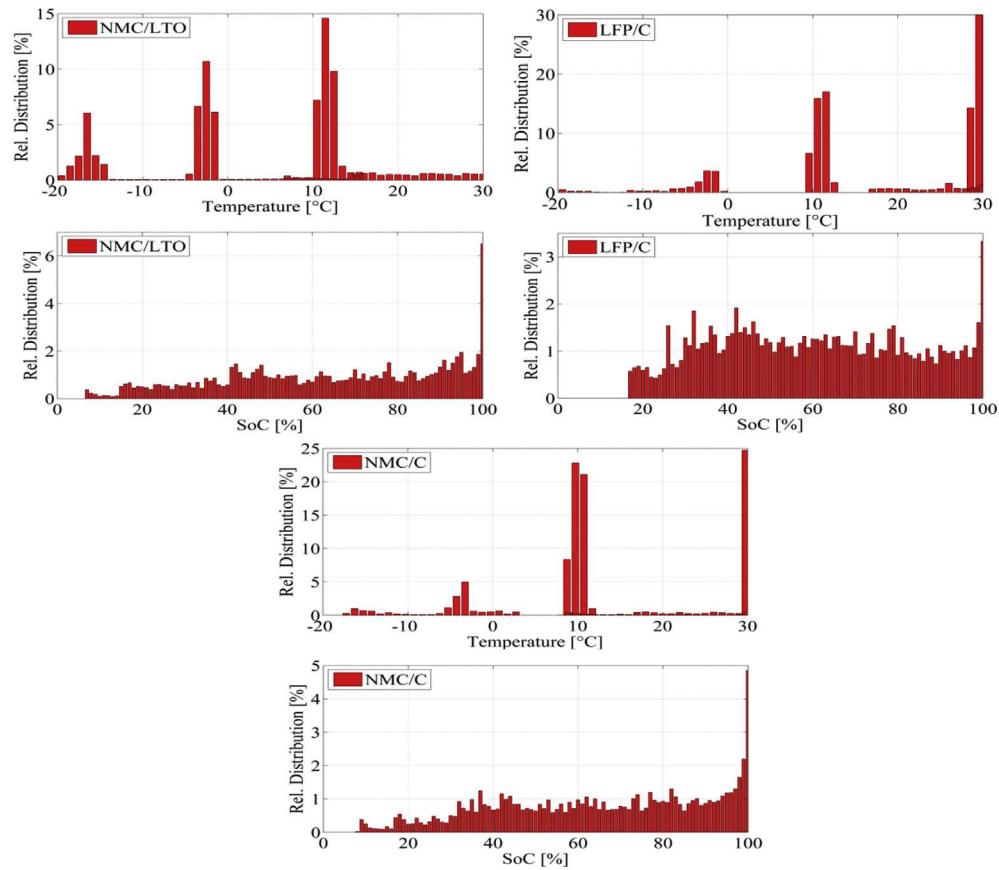
Fig. 3. Relative distribution of temperature and SoC of the employed driving cycles for each investigated LIB.
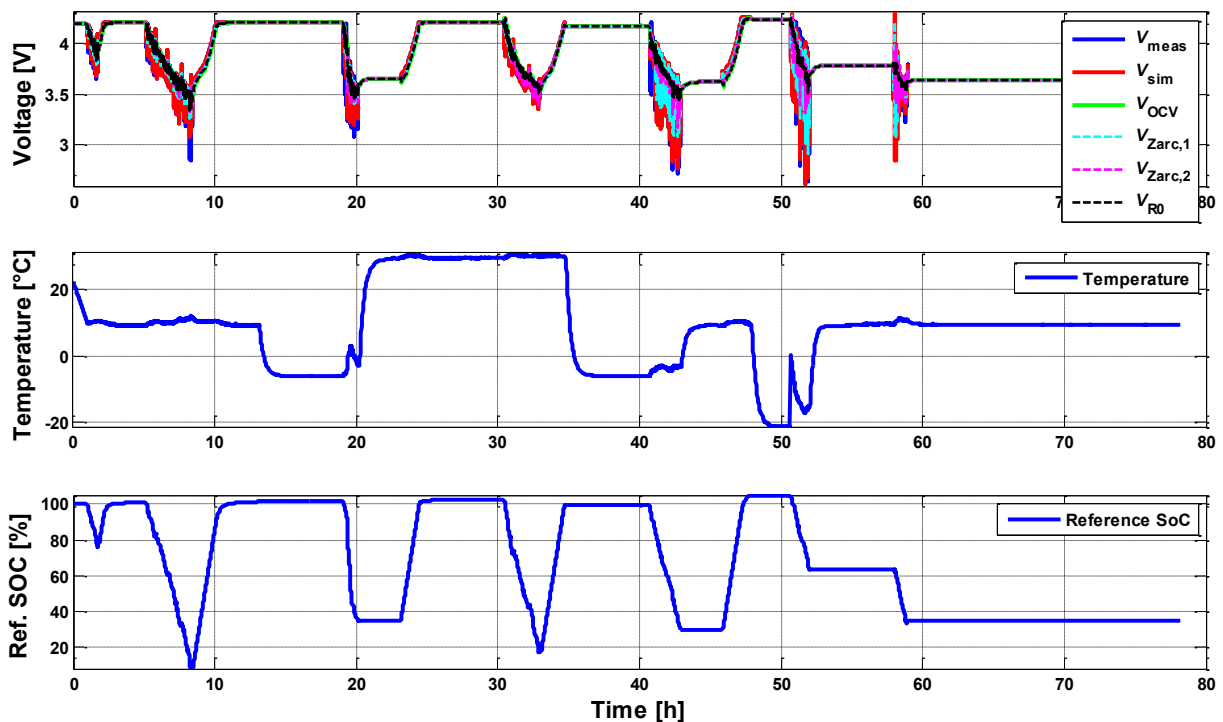

Fig. 4. Measured and simulated battery voltage (including determined overvoltages and OCV for 3 RC model), reference SoC and measured temperature of NMC/C LIB.
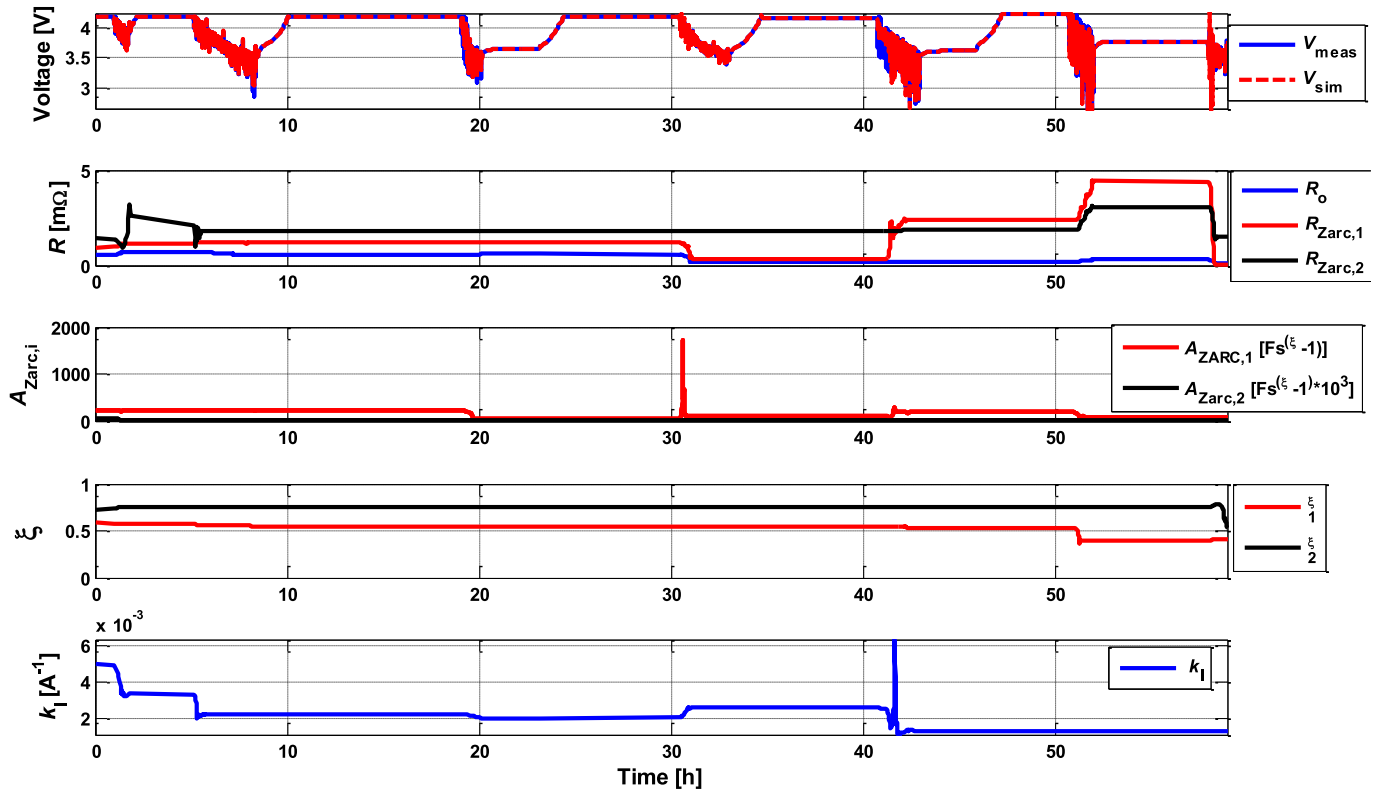
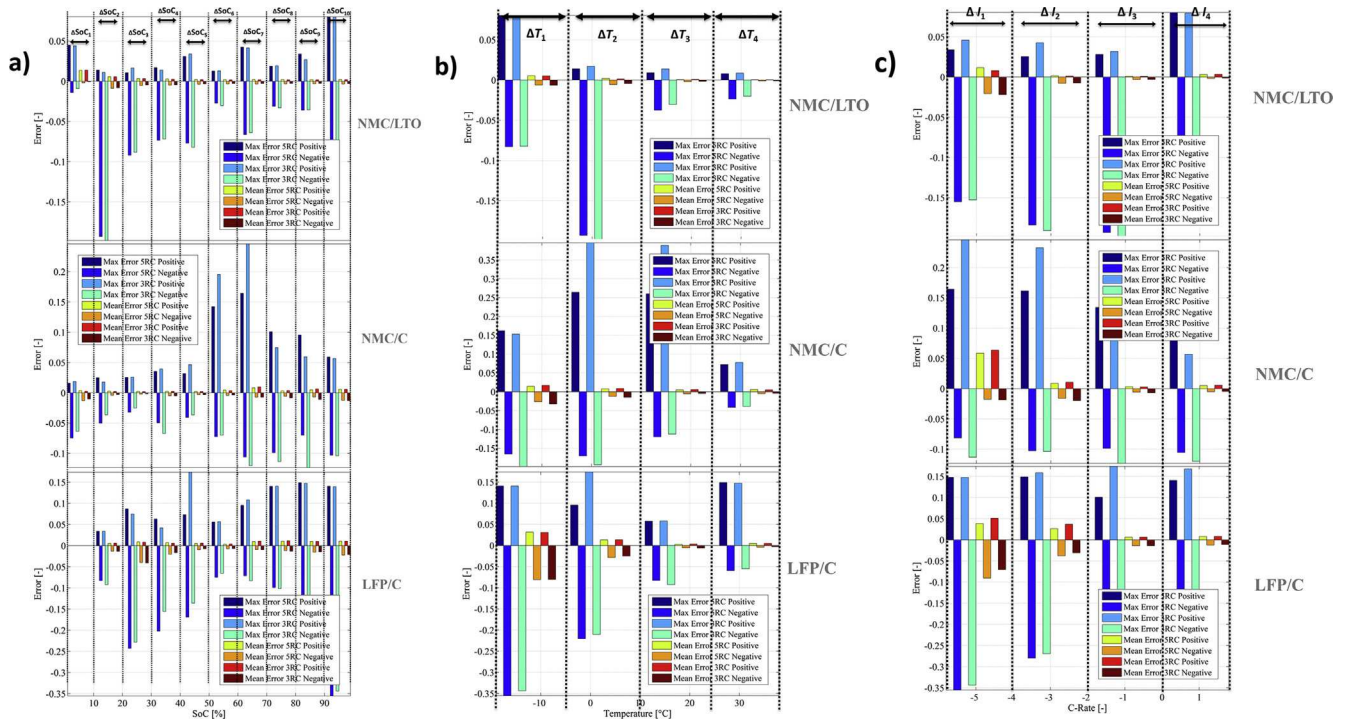**Fig. 5.** Results of applying the employed algorithm on NMC/C LIB for 3 RC model.

Fig. 6. Illustration of estimated minimum, maximum and mean battery voltage error (determined as described in Eq. 31) for: a) selected SoC ranges for investigated LIBs; b) selected temperature ranges of investigated LIBs; c) selected current ranges of investigated LIBs (please notice different scale of the graphs).

change of the OCV over SoC ($\Delta OCV/(I.t)$) can be considered additionally in Eq. (22).

As discussed before, actually the 5 RC model should be able to provide more accurate voltage estimation than the 3 RC model. However, after analyzing the error distribution it can be concluded that both of the models yield almost same accuracy.

4.2. Influence of temperature on voltage estimation

Impedance parameters are highly temperature dependent and change significantly with varying temperatures. Therefore, the examination of the influence of the temperature on the accuracy of the estimated battery voltage from ECM is necessary. The distribution of the voltage estimation error for predefined selected temperature ranges for each LIB is shown in Fig. 6b. Mean, minimum and maximum estimated voltage error for the following predefined temperature ranges and the mean voltage estimation error over a whole temperature range are determined:

- $\Delta T_1 = -20\ °C\ ...\ -5\ °C$
- $\Delta T_2 = -5\ °C\ ...\ 10\ °C$
- $\Delta T_3 = 10\ °C\ ...\ 25\ °C$
- $\Delta T_4 = 25\ °C\ ...\ 40\ °C$

As a result, while battery temperature is decreasing the estimation accuracy of the implemented ECM is increasing respectively. Estimation accuracy decreases by approximately a factor 2 with decreasing temperature of 10 K. This again indicates the high influence of LIB's temperature on the estimation accuracy of the battery model and shows the necessity of effective cooling system for battery pack and its consideration during development of battery state estimation algorithms.

4.3. Influence of current rate on voltage estimation

Moreover, the influence of applied current (current is given in C-Rate[2]) on estimation accuracy of the battery voltage is analyzed and the obtained results are illustrated in Fig. 6c. According to [10], applied load influences the estimation accuracy of the impedance parameters and estimated voltage respectively significantly. Mean, minimum and maximum determined errors of the estimated battery voltage are obtained by considering following selected current ranges:

- $\Delta I_1 <= -4C$
- $\Delta I_2 = -4C\ ...\ -2C$
- $\Delta I_3 = -2C\ ...\ 0C$
- $\Delta I_4 >= 0C$

By analyzing the obtained results, it becomes obvious that the estimation accuracy decreases with increasing discharge rate. Both ECMs provide almost the same accuracy with some low deviations, whereas a 5 RC model provides slightly better accuracy. Furthermore, due to the fact that for different current rates different electrochemical processes, such as reaction or diffusion processes are becoming more or less pronounced, it is interesting/necessary to examine and understand the influence of the applied current on the impedance characteristic of the investigated LIBs.

However, according to the results of the NMC/LTO LIB, it may be obtained that the influence of the current on the voltage estimation is less pronounced. This may be referred to the less pronounced impact of current dependence (as reported in our previous study [In review process]) of reaction processes of this LIB chemistry.

In Table 5, derived root-mean square error (RMSE) for each LIB over a whole driving cycle is given. It can be concluded that both ECMs yield almost the same level of accuracy in a range of below 100 mV with regard to the estimated voltage. The difference for all investigated LIBs is negligible so that the implementation of 3RC model due to its lower computational effort should be preferred. The same tendency can be observed when the mean estimated error over whole driving range is determined. Derived positive and negative mean errors are smaller than approx. 50 mV.

4.4. Adaptions analysis of the impedance parameters during an extreme temperature change over a wide SoC range

In the previous Section, the robustness analysis of the applied algorithm and applicability analysis of the used ECMs is performed. According to obtained results due to the high impact of the battery's temperature on the impedance characteristic, it is essential to ensure that the algorithm works accurately even when extraordinary internal or external battery temperature change occurs. For this reason, a measurement procedure on the test-bench is defined and the second day driving cycle from Fig. 2 is used again. The LIB was tempered in the temperature chamber for more hours to $-20\ °C$ at fully charged state. Then the test was performed, while the temperature was increased to $+30\ °C$ after 1 h driving until the battery was almost fully discharged and the driving cycle is ended. Fig. 7 shows exemplary the results for NMC/LTO LIB for both investigated ECMs.

As expected and shown in the previous section due to higher pronounced diffusion processes occurring in the battery at very low temperatures, in the beginning the deviation between estimated and measured voltage is higher than the estimated error when the temperature is increased. Furthermore, at very low SoCs the estimation accuracy decreases again due to discussed more pronounced diffusion phenomena and rapidly OCV change within this range as discussed above.

In Fig. 8 the adaption process of the ECM impedance parameters during the driving cycle is shown. The initial values of the parameters are intentionally chosen incorrect. The results indicate the fast adaption (approximately below 10 min) of the parameters to correct values for given conditions. For example, correct adaption of resistances can be seen while they are increasing with decreasing temperatures and decreasing with increasing temperatures respectively.

5. Conclusion

In this work an adaptive approach for on-board impedance parameters estimation while an impedance based battery model is applied is discussed. Presented approach is verified by employing a real seven day vehicle data from an electric vehicle prototype under temperature varying conditions and using LIBs at different aging states. Root-mean square error of estimated voltage of approximately less than 100 mV over whole driving cycles is achieved.

---

[2] C-Rate, corresponds to the current which needed to discharge the fully charged LIB when its nominal capacity is used as a reference. For an example, 1C current rate for a LIB with 40 Ah nominal capacity is equal to 40 A.
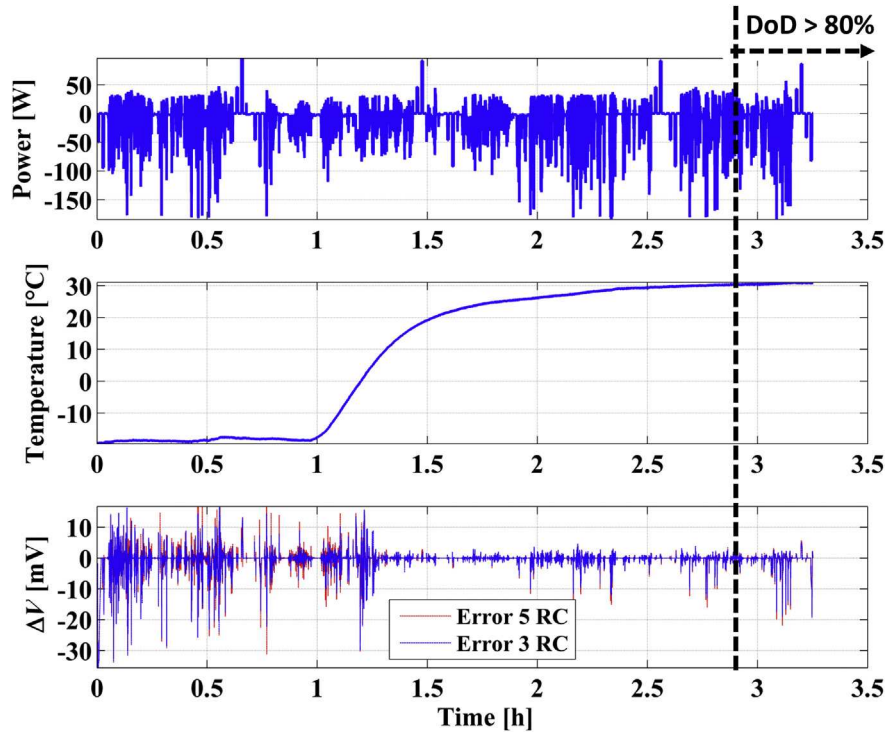
Table 5
Root-mean square error of estimated battery voltage for investigated LIBs over whole driving cycle.

	RMSE 3 RC model [mV]	RMSE 5 RC model [mV]
NMC/LTO	21.91	25.66
NMC/C	77.8	77.59
LFP/C	86.31	85.31

Fig. 7. Sensitivity analysis during an extreme temperature variation for both ECMs.
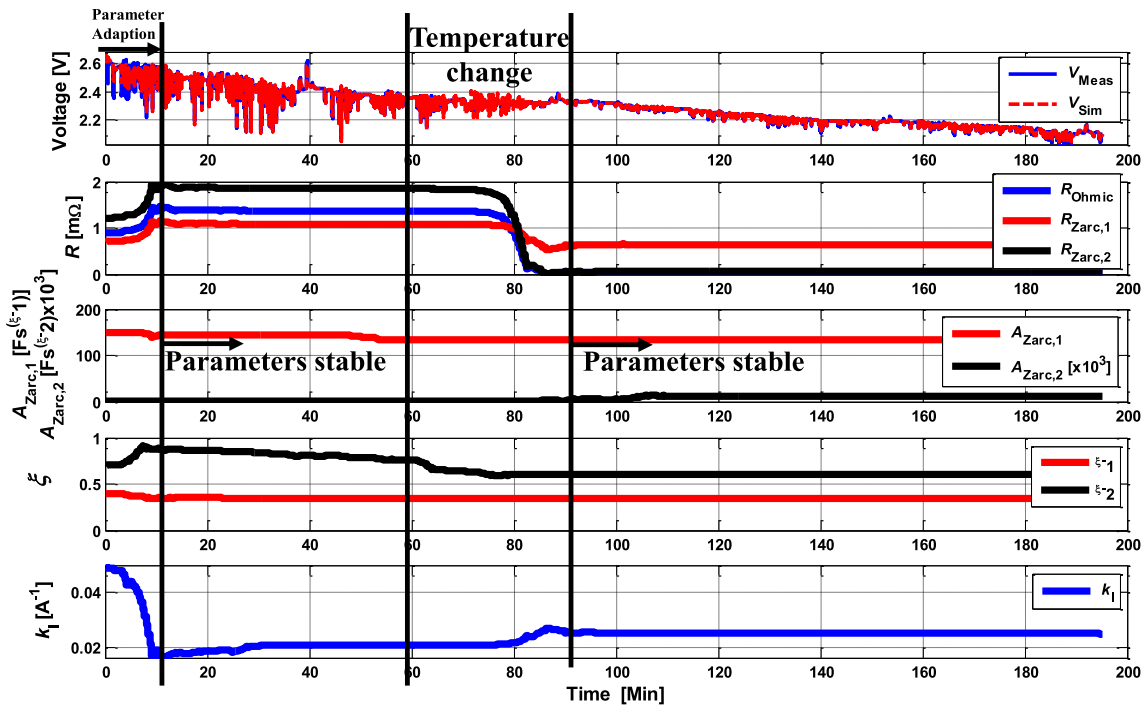

Fig. 8. Adaption analysis of the impedance parameters for 3 RC model investigating NMC/LTO LIB as a reference.

Furthermore, the influence of current, temperature and SoC on voltage estimation accuracy and the robustness of the proposed algorithm is approved.

Two equivalent circuit models approximating two ZARC-elements by finite number of RC-elements (3 RC model and 5 RC model) on-board are implemented and the possibility and advantageous of their implementation in embedded environment is shown. Adaptive nature of the applied algorithm and consideration

of the current dependence of the charge transfer resistance allows its implementation in applications such as EVs or HEVs in wide operating ranges.

Voltage estimation and robustness analysis of the algorithm indicate the higher and more reliable performance of 3RC model. Its simple implementation, its high long term robustness and low computational effort give the opportunity to employ it on a low-cost BMS with an aspect of larger accuracy.

In the next step, Hardware-in-the-loop (HIL) tests will be carried out for real-time applicability of the proposed approach. Based on the used algorithm, a novel technique employing a joint estimation filter for on-board states estimation, namely SoC and SoH will be presented in our future work.

Nomenclatures:

ACM	Adaptive Characteristic Map
AEKF	Adaptive extended Kalman filter
BMS	Battery management system
CDKF	Central difference Kalman filter
Dual EKF	Dual extended Kalman filter
DoD	Depth-of-Discharge
EKF	Extended Kalman filter
EIS	Electrochemical Impedance Spectroscopy
EV	Electric vehicle
ECM	Equivalent circuit model
EMS	Energy management system
HPPC	Hybrid Pulse Power Characterization
KF	Kalman filter
LIB	Lithium-ion battery
LFP	Positive electrode active materials with a common formula $LiFePO_4$
LS	Least square technique
LTO	Negative electrode active materials with a common formula $Li_4Ti_5O_{12}$
NMC	Positive electrode active materials with a common formula of $Li_x(Ni_xMn_yCo_z)O_2$
OCV	Open circuit voltage
PDE	Partial differential equation
RLS	Recursive least square
SP	Single particle model
SoA	State of the operating area
SoH	State-of-Health

SoC	State-of-Charge
SoF	State-of-Function
SPKF	Sigma point Kalman filter
UKF	Unscented Kalman filter
WRLS	Weighted recursive least square

Appendix A. Derivation of time-discrete model equations

Based on Eq. (1) and the definition of all over voltages and OCV, battery's voltage can be calculated as follows:

$$V_{Zarc,k_i}(t) = \sum_{k=1}^{2} \sum_{i=1}^{5\ or\ 3} V_{Zarc,k_i}(t) \tag{A.1}$$

$$V_{meas}(t) = V_{ocv}(t) + V_{R0}(t) + V_{Zarc,2}(t) + V_{Zarc,2}(t) \tag{A.2}$$

For $k = 1{:}2$ and $i = 1{:}3$ for 3 RC model and $i = 1{:}5$ for 5 RC model, then:

$$V_{Zarc,k_i}(t) = I(t) \cdot R_{Zarck,i} - R_{Zarck,i} \cdot V_{Zarc,k_i} \cdot \frac{dV_{Zarck,i}(t)}{dt} \tag{A.3}$$

Current dependence of the charge transfer resistance ($R_{Zarc,1}(I_R)$) as shown in Eq. (27) can simply be transformed to time-discrete domain:

$$R_{Zarc,1}(I_R) = R_{Zarc,0} \cdot \left(\frac{\ln\left(k_I \cdot I_R(k) + \sqrt{(k_I \cdot I_R(k))^2 + 1}\right)}{k_I \cdot I_R(k)} \right) \tag{A.4}$$

Eq. (A.2) can be directly transformed to time-discrete domain as follows:

$$V_{meas}(k) = V_{ocv}(k) + V_{R0}(k) + V_{Zarc,k_i}(k) + V_{Zarc,k_i}(k) \tag{A.5}$$

For Eq. (A.3) Laplace-transformation methodology can be employed:

$$V_{Zarc,k_i} = I(s) \cdot R_{Zarck,i} - s \cdot C_{Zarc,k_i} \cdot V_{Zarc,k_i}(s) \tag{A.6}$$

By using a bilinear transformation and some other simple mathematical transformation, following discretized equation can be obtained:

$$V_{Zarc,k_i} = \frac{Z^{-1} \cdot V_C(Z) \cdot \left(2R(I_R(Z)) \cdot \frac{C}{\Delta t} - 1\right) + R(I_R(k)) \cdot \left(I(Z) + Z^{-1} \cdot I(Z)\right)}{2 \cdot R(I_R(Z)) \cdot \frac{C}{\Delta t} + 1} \tag{A.7}$$

Now this can simply converted to the system consisting time step (k):

$$V_{Zarc,k_i} = \frac{U_{RC}(k-1) \cdot \left(R(I_R(k)) \cdot \frac{C}{\Delta t} - 1\right) + R(I_R(k)) \cdot (I(k) + I(k-1))}{2\Delta R(I_R(k)) \cdot \frac{C}{\Delta t} + 1} \tag{A.8}$$

References

[1] B. Scrosati, J. Garche, Lithium batteries: status, prospects and future, J. Power Sources 195 (no. 9) (2010) 2419–2430 [Online]. Available: http://www.sciencedirect.com/science/article/pii/S0378775309020564.

[2] L. Lu, X. Han, J. Li, J. Hua, M. Ouyang, A review on the key issues for lithium-ion battery management in electric vehicles, J. Power Sources 226 (no. 0) (2013)

272—288 [Online]. Available: http://www.sciencedirect.com/science/article// S0378775312016163.

[3] S. Rezvanizaniani, D. Liu, Y. Chen, J. Lee, Review and recent advances in battery health monitoring and prognostics technologies for electric vehicle (EV) safety and mobility, J. Power Sources 256 (no. 0) (2014) 110—124 [Online]. Available: http://www.sciencedirect.com/science/article/pii/S0378775314001098.

[4] T. Feng, L. Yang, X. Zhao, H. Zhang, J. Qiang, Online identification of lithium-ion battery parameters based on an improved equivalent-circuit model and its implementation on battery state-of-power prediction, J. Power Sources 281 (no. 0) (2015) 192—203 [Online]. Available: http://www.sciencedirect.com/ science/article/pii/S0378775315001706.

[5] S. Wang, M. Verbrugge, J.S. Wang, P. Liu, Multi-parameter battery state estimator based on the adaptive and direct solution of the governing differential equations, J. Power Sources 196 (no. 20) (2011) 8735—8741 [Online]. Available: http://www.sciencedirect.com/science/article/pii/S0378775311013152.

[6] S. Wang, M. Verbrugge, J.S. Wang, P. Liu, Power prediction from a battery state estimator that incorporates diffusion resistance, J. Power Sources 214 (no. 0) (2012) 399—406 [Online]. Available: http://www.sciencedirect.com/science/ article/pii/S037877531200804X.

[7] C. Fleischer, W. Waag, H.-M. Heyn, D.U. Sauer, On-line adaptive battery impedance parameter and state estimation considering physical principles in reduced order equivalent circuit battery models part 1. Requirements, critical review of methods and modeling, J. Power Sources 260 (2014) 276—291 [Online]. Available: http://www.sciencedirect.com/science/article/pii/ S0378775314002249.

[8] C. Fleischer, W. Waag, H.-M. Heyn, D.U. Sauer, On-line adaptive battery impedance parameter and state estimation considering physical principles in reduced order equivalent circuit battery models part 2. Parameter and state estimation, J. Power Sources 262 (2014) 457—482 [Online]. Available: http:// www.sciencedirect.com/science/article/pii/S0378775314003590.

[9] W. Waag, C. Fleischer, D.U. Sauer, "Critical review of the methods for monitoring of lithium-ion batteries in electric and hybrid vehicles, J. Power Sources 258 (no. 258) (2014) 321—339 [Online]. Available: http://www.sciencedirect. com/science/article/pii/S0378775314002572.

[10] W. Waag, Adaptive Algorithms for Monitoring of Lithium-ion Batteries in Electrical Vehicles, Ph.D. dissertation, ISEA-RWTH Aachen University, 2014, 978-3-8440-2976-5.

[11] O. Bohlen, Impedance-based Battery Monitoring, Ph.D. dissertation, RWTH Aachen University, 2008, 978-3-8322-7606-5.

[12] M. Kiel, Impedanzspektroskopie an batterien unter besonderer berücksichtung von batteriesensoren für den feldeinsatz, Ph.D. dissertation, RWTH Aachen University, 2013, 978-3-8440-1973-5.

[13] D. Howey, V. Yufit, P. Mitcheson, G. Offer, N. Brandon, Impedance measurement for advanced battery management systems, EVS 27 (2013).

[14] N. Chaturvedi, R. Klein, J. Christensen, J. Ahmed, A. Kojic, Algorithms for advanced battery-management systems, Control Syst. IEEE 30 (no. 3) (2010) 49—68.

[15] A.P. Schmidt, A Novel Electrochemical Battery Model for State of Charge and State of Health Estimation, Ph.D. dissertation, ETH, 2010.

[16] A.P. Schmidt, M. Bitzer, A.W. Imre, L. Guzzella, Model-based distinction and quantification of capacity loss and rate capability fade in Li-ion batteries, J. Power Sources 195 (no. 22) (2010) 7634—7638 [Online]. Available: http:// www.sciencedirect.com/science/article/pii/S0378775310009948.

[17] G.K. Prasad, C.D. Rahn, Model based identification of aging parameters in lithium ion batteries, J. Power Sources 232 (no. 0) (2013) 79—85 [Online]. Available: http://www.sciencedirect.com/science/article/pii/ S0378775313000700.

[18] W. Waag, S. Käbitz, D.U. Sauer, Experimental investigation of the lithium-ion battery impedance characteristic at various conditions and aging states and its influence on the application, Appl. Energy 102 (no. 0) (2013) 885—897 [Online]. Available: http://www.sciencedirect.com/science/article/pii/ S030626191200671X.

[19] D. Andre, M. Meiler, K. Steiner, C. Wimmer, T. Soczka-Guth, D. Sauer, Characterization of high-power lithium-ion batteries by electrochemical impedance spectroscopy. i. Experimental investigation, J. Power Sources 196 (no. 12) (2011) 5334—5341 [Online]. Available: http://www.sciencedirect.com/ science/article/pii/S0378775311000681.

[20] D. Andre, Systematic Characterization of Ageing Factors for High-energy Lithium-ion Cells and Approaches for Lifetime Modelling Regarding an Optimized Operating Strategy in Automotive Applications, Ph.D. dissertation, ISEA- RWTH Aachen, 2014, 978-3-8440-3587-2.

[21] J.E.B. Randles, Kinetics of rapid electrode reactions, Discuss. Faraday Soc. 1 (1947) 11—19 [Online]. Available: http://dx.doi.org/10.1039/DF9470100011.

[22] M. Ceraolo, New dynamical models of lead-acid batteries, Power Syst. IEEE Trans. 15 (no. 4) (2000) 1184—1190.

[23] F.M. Gonzalez-Longatt, Circuit based battery models: a review, IEEE Proc. (2006).

[24] X. Hu, S. Li, H. Peng, A comparative study of equivalent circuit models for Li-Ion batteries, J. Power Sources 198 (no. 0) (2012) 359—367 [Online]. Available: http://www.sciencedirect.com/science/article/pii/S0378775311019628.

[25] G.L. Plett, Extended kalman filtering for battery management systems of LiPB-based hev battery packs: part 3. State and parameter estimation, J. Power Sources 134 (no. 2) (2004) 277—292 [Online]. Available: http://www.sciencedirect.com/science/article/pii/S0378775304003611.

[26] D.V. Do, C. Forgez, K. El Kadri Benkara, G. Friedrich, Impedance observer for a Li-ion battery using Kalman filter, Veh. Technol. IEEE Trans. 58 (no. 8) (2009) 3930—3937.

[27] J. Remmlinger, M. Buchholz, K. Dietmayer, Model-based on-board monitoring for lithium-ion batteries, ATZ Autom. 62 (4) (2014) 282—295, http:// dx.doi.org/10.1515/auto-2013-1046.

[28] J. Remmlinger, M. Buchholz, M. Meiler, P. Bernreuter, K. Dietmayer, State-of-health monitoring of lithium-ion batteries in electric vehicles by on-board internal resistance estimation, J. Power Sources 196 (no. 12) (2011) 5357—5363 [Online]. Available: http://www.sciencedirect.com/science/ article/pii/S0378775310013534.

[29] J. Remmlinger, M. Buchholz, T. Soczka-Guth, K. Dietmayer, On-board state-of-health monitoring of lithium-ion batteries using linear parameter-varying models, J. Power Sources 254 (2014) 268—276, http://dx.doi.org/10.1016/ j.jpowsour.2013.12.101.

[30] G.L. Plett, Extended Kalman filtering for battery management systems of LiPB-based HEV battery packs: part 1. Background, J. Power Sources 134 (no. 2) (2004) 252—261 [Online]. Available: http://www.sciencedirect.com/science/ article/pii/S0378775304003593.

[31] G.L. Plett, Extended kalman filtering for battery management systems of LiPB-based HEV battery packs: part 2. Modeling and identification, J. Power Sources 134 (no. 2) (2004) 262—276 [Online]. Available: http://www.sciencedirect. com/science/article/pii/S037877530400360X.

[32] G.L. Plett, Sigma-point kalman filtering for battery management systems ofLIPB-based HEV battery packs: part 1: introduction and state estimation, J. Power Sources 161 (no. 2) (2006) 1356—1368 [Online]. Available: http:// www.sciencedirect.com/science/article/pii/S0378775306011414.

[33] G.L. Plett, Sigma-point kalman filtering for battery management systems of LIPB-based HEV battery packs: part 2: simultaneous state and parameter estimation, J. Power Sources 161 (no. 2) (2006) 1369—1384 [Online]. Available: http://www.sciencedirect.com/science/article/pii/S0378775306011438.

[34] W. Waag, C. Fleischer, D.U. Sauer, On-line estimation of lithium-ion battery impedance parameters using a novel varied-parameters approach, J. Power Sources 237 (no. 0) (2013) 260—269 [Online]. Available: http://www. sciencedirect.com/science/article/pii/S0378775313004254.

[35] S. Buller, Impedance-based Simulation Models for Energy Storage Devices in Advanced Automotive Power Systems, Ph.D. dissertation, Institute for Power Electronics and Electrical Drives, RWTH Aachen University, 2003, 978-3-8322-1225-4.

[36] E. Barsoukov, J.R. Macdonald, Impedance Spectroscopy, Wiley, 2005, 0-471-64749-7.

[37] J. Kowal, Spatially-resolved Impedance of Nonlinear Inhomogeneous Devices - using the Example of Lead-acid Batteries, Ph.D. dissertation, ISEA, 2010, 978-3-8322-9483-0.

[38] C.Y.-W. Christopher, D. Rahn, Battery Systems Engineering, WILLEY, 2013, 9781119979500.

[39] D. Bendt, Maintenance-free Batteries, Research Studies Press LTD, 2003, 0 86380 279 6.

[40] A. Jossen, W. Weydanz, Moderne Akkumulatoren richtig einsetzen, 2006 [Online]. Available: http://books.google.de/books?id=fTidMQAACAAJ.

[41] D. Linden, T.B. Reddy, Handbook of Batteries, 2002, 0-07-135978-8.

[42] T. Erey-Gruz, M. Volmer, The theory of hydrogen high tension, J. Phys. Chem. 150 (1930) 203—213.

[43] M.A. Roscher, Zustandserkennung von lifepo4 -batterien für Hybrid- und Elektrofahrzeuge, Ph.D. dissertation, RWTH Aachen University, 2010, 978-3-8322-9738-1.

[44] Y. Xing, W. He, M. Pecht, K.L. Tsui, State of charge estimation of lithium-ion batteries using the open-circuit voltage at various ambient temperatures, Appl. Energy 113 (no. 0) (2014) 106—115 [Online]. Available: http://www. sciencedirect.com/science/article/pii/S0306261913005746.

[45] J.P. Schmidt, Verfahren zur Charakterisierung und Modellierung von Lithium-Ionen Zellen, Ph.D. dissertation, KIT, 2013.